In-situ hydrothermal synthesis of zinc oxide nanostructures using microheaters

Wei-Chih Lin, Yu-Ching Lin, Masayoshi Esashi, and Ashwin A. Seshia

Abstract—A technique for in-situ hydrothermal synthesis of transversely suspended zinc oxide nanowires (ZnO NWs) using microfabricated heaters is presented. A number of issues relating to seed layer preparation, directed alignment, local heating control and the concentration of the synthesis solution are investigated for this method. It is shown that ZnO NWs can be synthesized and aligned from the ZnO seed surface to bridge two adjacent microheater elements. Moreover, hybrid ZnO nanotubes and nanorods are also synthesized by controlling the concentration of the synthesis solution employed. The crystalline structure of synthesized ZnO nanostructures are characterized by the transmission electron microscope (TEM) and selective area electron diffraction (SAED). Finally, ZnO NW devices based on proposed microheater synthesis approach are characterised for UV photoresponsivity demonstrating the potential of this approach to address practical device applications.

Index Terms—Zinc oxide nanostructures, microheaters, local nanostructure synthesis, hydrothermal synthesis and UV photodetector.

I. INTRODUCTION

A variety of research has reported the performance of one-dimensional (1D) ZnO NW devices based on exceptional device properties[1]. The piezoelectric, optical and semiconducting properties of ZnO nanowires have been utilised to create electrically actuated high frequency nanowire resonators[2], transistors, chemical sensors and energy harvesting devices. The most commonly adopted approach for fabricating ZnO nanowires is the Remove-Disperse-Align technique[3]. In this method, ZnO NWs are first separately synthesized on a growth substrate and then trans-located onto a device substrate. In most instances, this process requires precision pick-and-place alignment or other directed assembly techniques to integrate the nanowires onto specific locations for device applications[4]. Previous work has demonstrated the possibility of synthesizing transversely grown ZnO NWs directly on SOI substrates[5]. In this approach the nanowires

were grown in a furnace at 800-915°C using the vapor-solid approach using an ALD deposited thin-film ZnO seed layer. However, in applications requiring co-integration of nanowires together with CMOS, the high temperatures required for synthesis may not be compatible with the material stack on the device substrate.

A number of methods to integrate top-down[6] and bottom-up[7] nanofabrication approaches[4] have been proposed to address these technical limitations. Among the approaches proposed, the integration of local synthesis or directed alignment has been previously realized by using microfabricated devices. Microheater units [8] can be utilised in the MOCVD synthesis process for synthesizing ZnO nanostructures[9] – however, this still exposes the chip to high temperatures during the synthesis process. To avoid high temperature synthesis, CVD combined with a laser ablation approach has been studied for the fabrication of ZnO nanostructures at low temperature and low pressure [10]. ZnO nanostructures grown by using wet chemical synthesis processes have also been previously employed and previous work includes a room ambient sonochemical process to synthesize ZnO nanowires for fabricating UV photodetectors and gas sensors on amorphous substrates [11]. Similarly, other research reported directional control by using dielectrophoresis-driven assembly to position nanoparticles for ZnO NWs growth by low temperature hydrothermal synthesis [12]. Both presented methods show that the *in-situ* technique based on microfabricated reactor elements has potential to precisely control and synthesize nanomaterials for fabricating nanowire devices.

In this paper, we report a simple and repeatable ZnO NWs synthesis and alignment approach in aqueous solution using platinum (Pt) planar microheaters [13]. Fig. 1 (a) provides a schematic illustration of the ZnO NWs synthesis device. As shown in Fig. 1 (b), each device on this platform consists of a pair of microheaters, composed of an electroresistive Pt layer, connected with two separate conductive gold (Au) wires. The input power can be applied via the Au conductive wire to the Pt electroresistive microheater to generate local heating for forming an oxidised ZnO seed layer and synthesising ZnO NWs as illustrated in Fig. 1 (c) and (d). Fig. 1 (c) presents the first step and the Zn layer is oxidized using microheaters located directly below the layer in the ambient environment. Then, horizontally grown ZnO NWs emerge from the sidewall of the oxidised ZnO seed surface based on the same local heating under a hydrothermal synthesis approach, as illustrated in Fig. 1 (d). During the synthesis process, a combination of electric field and SiO_2 constraining layer directed alignment is utilised to control the direction of

nanowire growth. We propose that this method has the potential to rapidly and locally synthesize nanostructures *in-situ* on silicon substrates without the need for assembly processes.
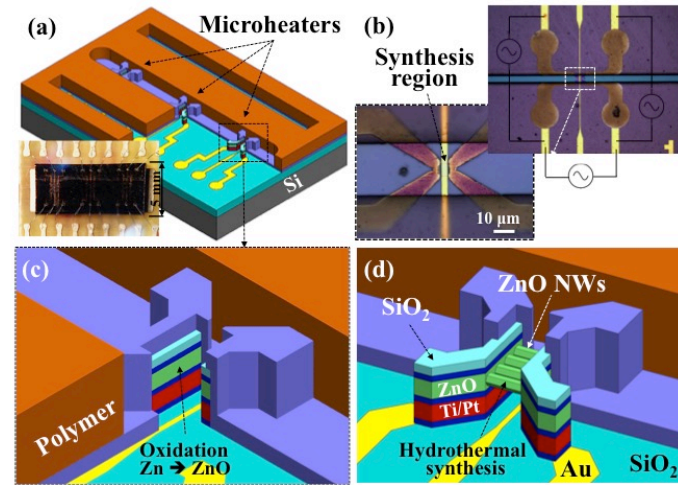

Fig. 1 (a) Illustration of the ZnO NW synthesis device; (b) Optical pictures of the fabricated microheater device; (c) Illustration of the oxidation process for forming ZnO seed layer and (d) Illustration of ZnO NWs synthesis by using hydrothermal synthesis.

II. EXPERIMENTAL DETAILS

Nanowire synthesis is governed by factors that include the energy input required for synthesis, precursor materials for growth, and defining the growth texture of the substrate. To obtain a desired nanofabricated device with defined geometry, morphology and material properties, these parameters have to be controlled precisely during the synthesis process. For example, in hydrothermal synthesis, the morphology, length and diameter of synthesized ZnO NWs are mainly influenced by the reactant concentration (precursor), heating temperature (synthesis energy) and surface conduction of seed layer (growth texture). In this research, the growth of ZnO NWs is based on the hydrothermal synthesis method. For synthesising well-controlled geometries of ZnO nanostructures, optimisation of the growth parameters for hydrothermal synthesis is necessary [14]. Therefore, several issues, including the condition of the seed layer and local heating, are studied to discover optimized synthesis parameters as described below.

A. Fabrication and characterisation of microheaters

Microheater Fabrication. Several microfabrication processes were utilized to construct the microheater devices and the fabrication process is illustrated sequentially in Fig. 2 (a) to (h). As described previously [15], the process commences with fabricating the Cr/Au conductive wires as shown in Fig. 3 (a). The thickness of Cr and Au layer are around 20 and 200 nm, respectively. The conductive Au wire is embedded within the SiO_2 layer to eliminate the step coverage effect. Then, photolithography and dry processes are utilized to pattern the multilayer, including Ti, Pt, Cr, Zn and SiO_2, for microheater fabrication, as illustrated in Fig. 2 (b) and (c). Similar processes were repeated to produce the cover layer for isolating the synthesis solution from contact with
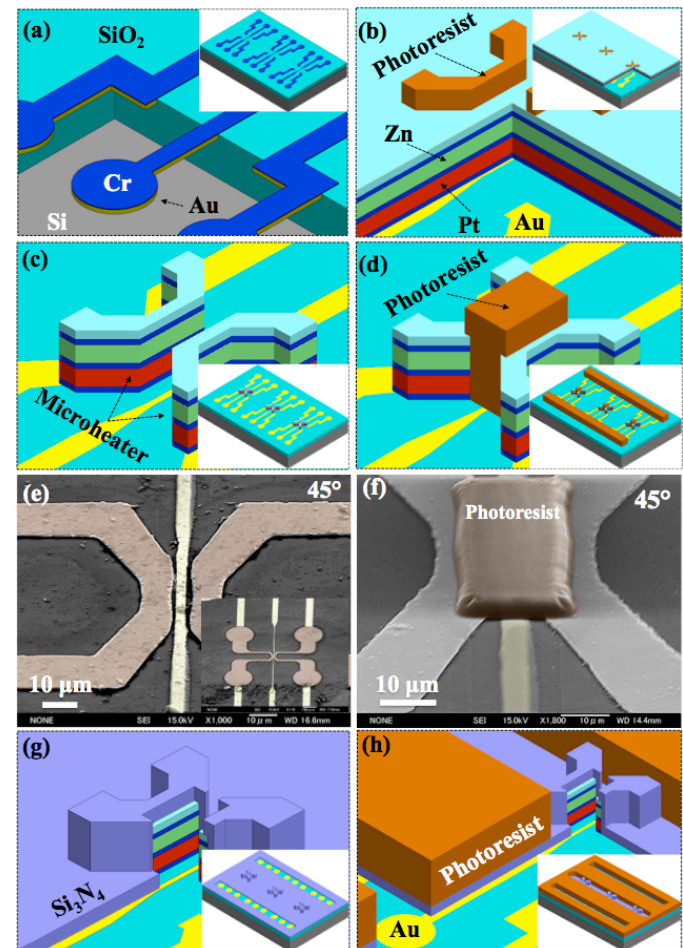
microheaters.

Fig. 2 (a)-(h): Schematic description and SEM images of the fabrication sequence for the microheater array.

Characterization of Microheaters. In conventional hydrothermal synthesis, a synthesis temperature of 90 °C is frequently used for ZnO NWs. In this work, the microheater devices are first characterized to establish a temperature-power database to meet this requirement. The microheater devices are operated by applying voltages from 0 V peak-to-peak (V_{pp}), 10 kHz to 10 V_{pp} at a voltage ramp rate of 0.1 V/sec under ambient conditions. An infrared camera (TVS-500EX, NEC) with 18.5 µm mapping resolution and microlens is used to measure the generated temperature profile. The chip was placed on a commercial XYZ stage under ambient environment and measurements were conducted inside a light-insulated enclosure. Fig. 3 (b-d) shows measured temperature distribution images by applying 4, 6 and 10 V_{pp} and the results for temperature distribution in the microheater zone are then tabulated. As can be seen from the measured temperature distribution, due to a high thermal conductivity of Pt and Au materials, the generated heat is rapidly conducted to the entire microheater surface and to the Au conductive wires. However, this issue can be partly mitigated by adopting low thermal conductivity constraining layers such as SiO_2 or Si_3N_4. Therefore, ZnO NWs are only synthesized at the edge of the microheaters as a result.
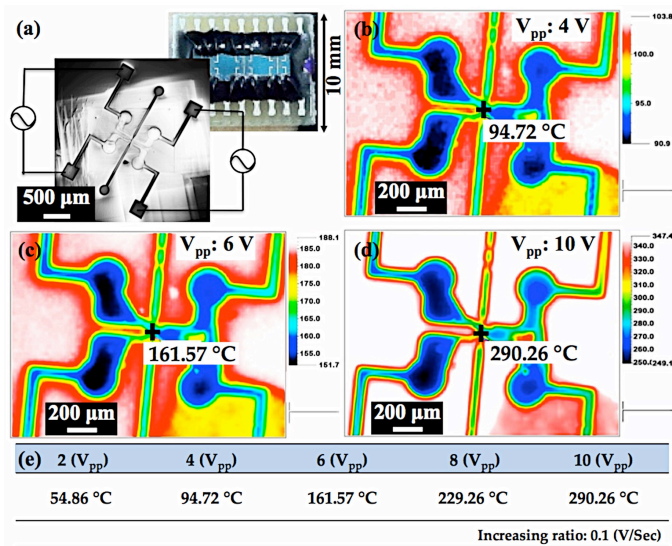
Fig. 3 (a) The packaged chip and device unit; (b-d) Temperature distribution images measured for various applied voltages and (e) table showing the temperature.

B. Growth-texture seed layer

Numerous seed layer materials have been previously utilised to provide the necessary conditions for nanostructure synthesis. The roles of the seed layer material are to provide the starting textured substrate as a grain-growth template for nanostructure synthesis. Normally, the geometries of the synthesized 1D nanostructures are based on the growth surface condition of the seed layer, such as the grain size, grain distribution, grain boundary and deposited surface roughness and uniformity. Nanostructures are basically grown from the grains of the seed layer so that the diameters of nanostructures are determined by the surface conditions of deposited seed layers. Our previous experiments show that the smaller the size of the nucleated ZnO seeds, the thinner the diameter of the synthesized ZnO NWs [16]. On the other hand, the desired crystallographic orientation can be determined by the seed layer and this crystallographic orientation can provide an epitaxial growth surface condition during nanostructure synthesis. Then, the nanostructures are synthesized along with this determined growth orientation.

Deposition of the Zn layer. In the hydrothermal synthesis approach, ZnO (in nanoparticle and thin film formats), are commonly utilised as seed layers for ZnO NWs synthesis. In this paper, we proposed an oxidation method using microheaters to form a suitable epitaxial growth surface and create fine grains of nucleated ZnO seeds for ZnO NW synthesis [16]. The first step is to deposit a Zn layer on the Pt microheater layer. By considering two mentioned requirements, a fine grained and desired crystallographic orientation on a smooth seed layer surface is necessary. Several deposition conditions are studied for a good quality Zn layer. The employed RF sputtering powers commenced from 45 W up to 300 W under 0.5 Pa chamber pressure and 8 sccm of Ar gas. The deposition rate and surface roughness relative to the sputtering power are shown in Table 1. The average thickness of the deposited Zn layer was measured from three selected positions on five different samples and the total deposition time was 3 minutes. The surface roughness of the deposited Zn layer was measured using the AFM that showed a decrease in surface roughness with decreasing sputtering power. The average roughness (Ra) of the Zn layer is 91 (300 W), 45.3 (200 W), 30.2 (100 W), 22.6 (70 W), 16.0 (60 W) and 15.6 nm (45 W) following measurements using an AFM.

Table. 1 The deposition ratio and surface roughness of Zn layer as functions of different sputtering powers.

Power (W)	Deposition rate (nm/min)	Surface roughness (nm)	
300	448	Ra: 91.0	Rq: 119
200	211	Ra: 45.3	Rq: 52.2
100	91	Ra: 30.2	Rq: 30.6
70	69	Ra: 22.6	Rq: 27.1
60	51	Ra: 16.0	Rq: 22.9
45	47	Ra: 15.6	Rq: 24.2

Figure 4 (a-d) shows the surface morphology of each deposited Zn layer using 300 W, 100 W, 70 W and 45 W sputtering powers, respectively. As can be seen from Fig. 4 (a) and (b), the SEM pictures clearly show that the shape of the grain size is hexagonal which means the Zn layer is oxidised during the deposition. There is no hexagonal ZnO structure synthesised by using the 70 W and 45 W deposition power as shown in Fig. 4 (c) and (d).
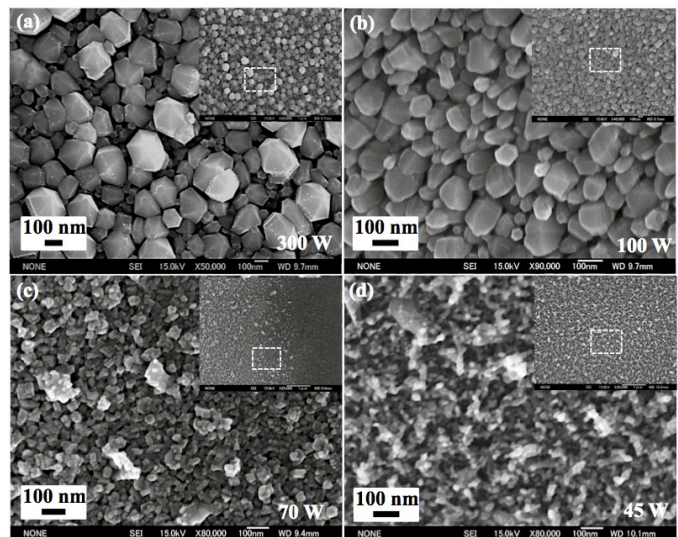

Fig. 4 The surface morphology of the deposited Zn layer for (a) 300 W, (b) 100 W, (c) 70 W, and (d) 45 W of sputtering power.

To investigate the hexagonal structure, we utilised the Raman Spectrum to identify the layers, which are deposited by using 300 W and 200 W powers, where there are two broad peaks presented in the range of 300-450 and 550-600 cm^{-1}, as presented in the corresponding measurement shown in Fig. 5. These regions attribute to ZnO peaks [17] which are E_2(high) 438 cm^{-1}, A_1(high) 381 cm^{-1}, A_1(TO) 378 cm^{-1}, E_1(TO) 409 cm^{-1}, A_1(LO) 571 cm^{-1}, A_1 (2LA) 483 cm^{-1}, E_1(LO) 583 cm^{-1} and E_2(TO) 335 cm^{-1}. The Raman peaks at 483 cm^{-1} is associated with the A_1 (2LA) mode of ZnO signal and is prominently seen in the green (300 W) and yellow line (200 W) respectively. This clearly corresponds to the ZnO nanorods and oxidation might be occurred during the deposition process. Similarly, the Zn layer deposited at 100 W power still

shows evidence of oxidised ZnO nanostructures and also some low signal peaks (blue line) revealed in these two regions. Therefore, the applied sputtering power to deposit the Zn layer should be less than 100 W. This also can be supported by the measured Raman spectrums and the sputtering power of 70 (red line) and 45W (black line) have a smooth and obvious Zn peak at 566 cm^{-1} and there is no obvious ZnO peaks revealed for these cases.
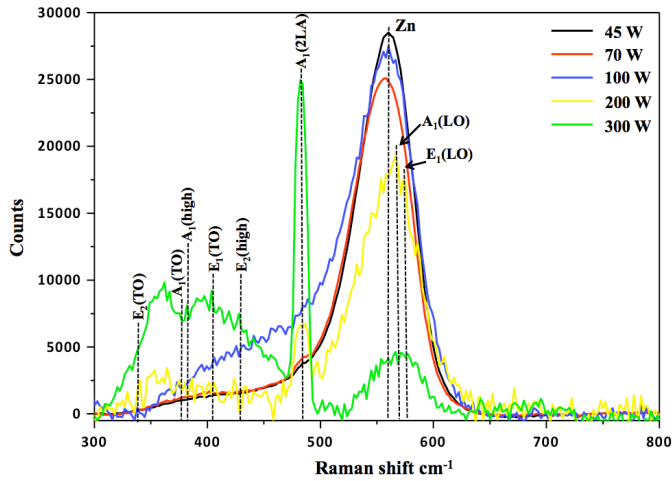

Fig. 5 Raman spectrum for the Zn layers deposited by different sputtering powers corresponding to the cases shown in Table 1. and Fig. 4.

Although decreasing the sputtering power can reduce the growth of oxidized ZnO NWs during the deposition process, low deposition power does not enable sufficient adhesion for the deposited Zn layer. As revealed in Fig. 6 (a, c and d), the initial Zn layer deposited by using 40 W sputtering power was oxidized by applying an 8 V (0.8 W) heating voltage and 30 V bias voltage between two microheaters to form the ZnO seed layer. However some catenarian Zn nanostructures, confirmed through SEM and EDS, as seen from the images in Fig 5 (a-b), form between two microheaters after the oxidation process. Zn nanoparticles might move from the deposited Zn layer and locate in the ground substrate driven by the electric field. To consider the trade-off between the issues of oxidation and adhesion, a sputtering power of 70 W was utilised for the Zn layer deposition in this research.
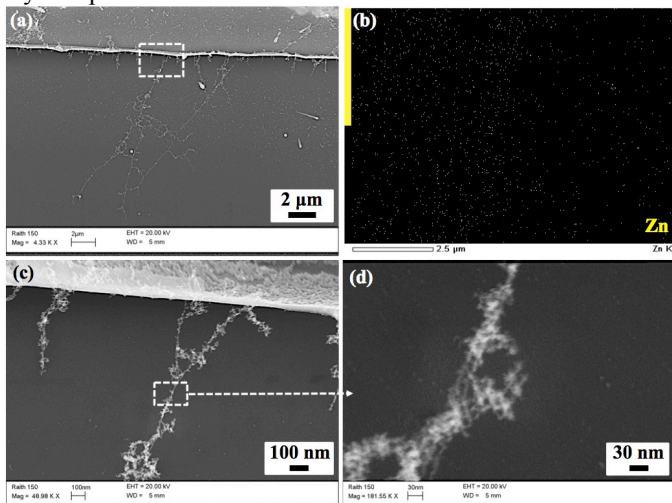

Fig. 6 (a-d) SEM and EDS pictures of synthesized catenarian ZnO NWs following an oxidation and alignment process.

Preparation of oxidised ZnO seed layer. Fig. 7 (a) presents the formation of oxidized ZnO seed layer by operating the microheaters under ambient conditions. The reaction of zinc ions and oxygen starts from the Zn top surface progressing to the bottom of the layer. By using this method, the fine grain size and ZnO nuclei can be grown on the surface of the oxidised ZnO layer. This research investigated oxidation of a variety of Zn layer thicknesses, ranging from 50 nm to 500 nm. Then, we tested the oxidized ZnO seed layer under hydrothermal synthesis methods for locally growth ZnO NWs. Fig. 7 (b-c) demonstrates two different thicknesses of ZnO seed layers that are oxidised by applying 10 V_{pp}, 10 kHz under ambient conditions for 10 minutes. Next, the whole device is immersed into 20 mM of zinc nitrate and HMTA solution and 4 V_{pp}, 100 kHz heating voltages are applied to the microheaters for 90 minutes to synthesize the ZnO NWs. As can be clearly seen from the SEM pictures in Fig. 7 (b-c), ZnO NWs are fully grown and uniformly synthesized onto the entire oxidised ZnO seed surface. Therefore, this experimental result proves that oxidation by using a microheater-based approach is feasible. An oxidised ZnO seed layer with nanoscale features can be also achieved by this proposed microheater-heating method.
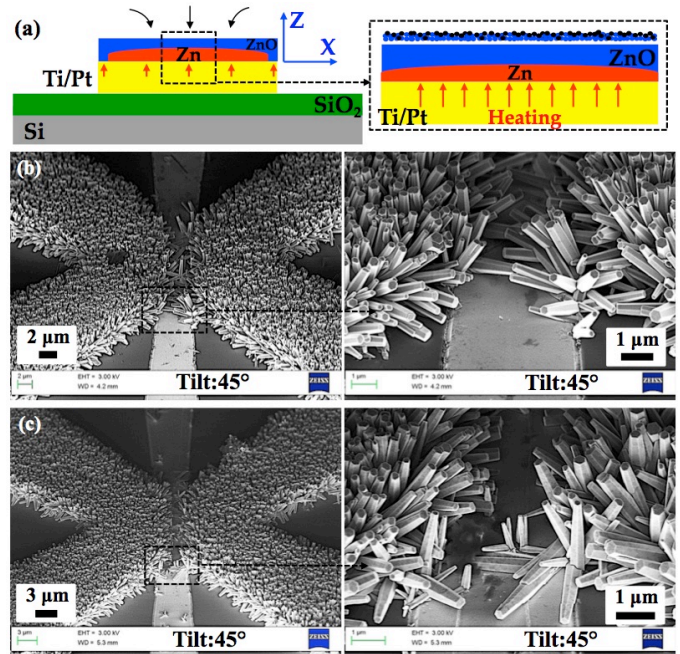

Fig. 7 (a) The illustration of the oxidation procedure and (b-c) show SEM images of synthesized ZnO NWs by a local aqueous heating method after Zn oxidation.

C. Synthesis of transversely suspended ZnO NWs

Constraining layer. In this work, various thicknesses of SiO$_2$, ranging from 25 nm to 500 nm, are deposited onto the oxidised Zn layer as a constraining layer for controlling the growth direction. The SiO$_2$ constraining layer is utilized to prevent the growth of ZnO NWs in the vertical direction. The topside of the Zn surface is isolated from the synthesis solution so that ZnO nanostructures are only synthesized on the exposed sidewall area. Fig. 8 from (a) to (d) show SEM images of the oxidised ZnO seed layer covered by a 25 nm, 50 nm and 100 nm thick SiO$_2$ layer and the oxidation follows the

same process as presented in Fig. 7 (b-c). Then, these devices are dipped into the synthesis solution for 2 hours for synthesis by the conventional hydrothermal method. As can be seen from Fig. 8 (b-c), 25 nm and 50 nm thick SiO_2 does not provide sufficient isolation to prevent ZnO NWs synthesis. The SiO_2 layer is peeled off by synthesized ZnO NWs that may result due to a non-conformal SiO_2 layer deposition and pinholes present in the constraining layer. The synthesis solution can react with ZnO seed layer via these pinholes to grow ZnO NWs ultimately resulting in peeling off the entire SiO_2 layer. A 100 nm thick SiO_2 layer is sufficiently constraining and is found to prevent ZnO NWs synthesis in the vertical direction as shown in Fig. 8 (d). The ZnO NWs grow on the sidewall region of the oxidised ZnO seed surface in this case.
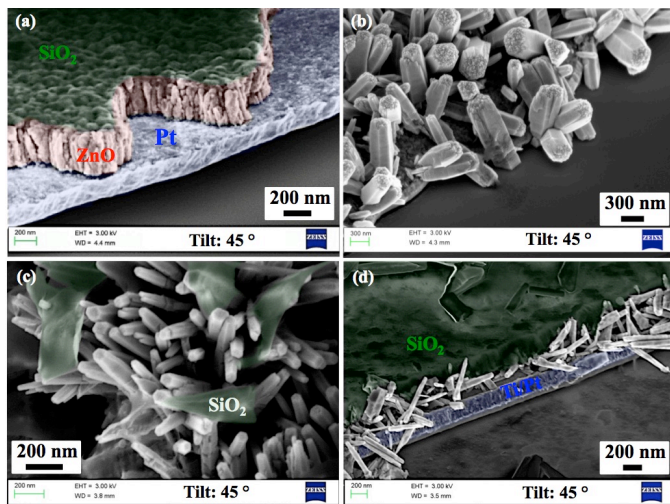

Fig. 8 (a) The initial Zn layer covered by a constraining SiO_2 layer; (b) and (c) The identification of the thickness of constraining SiO_2 layer for preventing ZnO NWs synthesis.

Electric field assistance. A further alignment approach is to set up an electric field to control the direction of nanowire growth between the two microheaters during the synthesis process. By using the parameters discussed above, the device covered by a 100 nm constraining SiO_2 layer is first oxidised to form a ZnO layer and dipped into the synthesis solution. Next, the heating voltage is set to $6V_{pp}$ applied between the two microheaters and the frequency is varied 10 kHz, as shown in Fig. 2, to the left microheater. The 6 V_{pp} bias voltages with a set of frequency, including 10 kHz, 100 kHz, 1 MHz and 10 MHz, are applied between two microheaters. Fig. 9 (a) and (b) show the synthesized ZnO NWs by applied $6V_{pp}$, 10 kHz and $6V_{pp}$, 1 MHz bias voltages, respectively. As can be seen from the SEM pictures, the ZnO NWs growth starts from the left side to bridge the gap between two microheaters after 50 minutes. The higher the frequency of the applied bias voltage the smaller diameter of the resulting nanowires.

Although the above experiment shows that the 100 nm SiO_2 constraining layer can prevent vertical ZnO NWs synthesis, there is still some peeling of the constraining layer that is observed. Therefore, the heating voltage is decreased to $4V_{pp}$ 10 kHz and the bias voltage is increased to 10 V_{pp}, 10 MHz. However, ZnO nanostructures are still gradually grown on the top surface of microheaters during an hour synthesis, as

shown in Fig. 7 (c). Then the synthesized ZnO nanostructure aggregates to a ZnO ball with an emerged single ZnO NW.
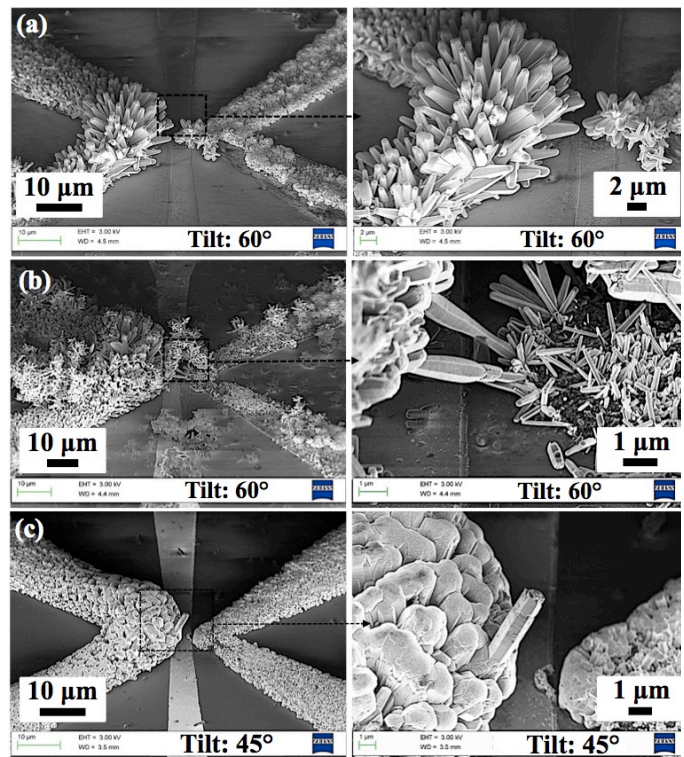

Fig.9 (a-c) Synthesized ZnO NWs by applying fixed 6 Vpp bias voltages at various frequencies including 10 kHz, 1 MHz and 10 MHz.

III. RESULTS AND DISCUSSION

Testing of oxidized seed layer in the sidewall region. The thickness of the constraining SiO_2 layer is increased to 500 nm for a further series of experiments. The Zn layer is oxidised to create the ZnO seed layer in a manner identical to the earlier protocol. The diffusion of oxygen and zinc ions starts from the uncovered sidewall of the Zn surface and then the oxidised ZnO seed layer is created, as illustrated in Fig. 10 (a). After a 10 minute oxidation process, few regions of constraining SiO_2 are randomly removed by physical etching. Next, the whole device is dipped into the synthesis solvent and the $4V_{pp}$ 10 kHz heating voltage is applied to the both microheaters for 15 minutes synthesis. As can be seen in Figs. 10 (b) - (e), ZnO NWs grow only on the sidewalls and oxidised ZnO areas where the constraining SiO_2 has been removed. Furthermore, it clearly shows that the density of synthesized ZnO NWs in the apex part of the microheater is decreased from the tip to the root regions of the electrodes. This clearly is qualitatively consistent with the fact that the density of ZnO NWs is based on the applied heating voltages and times, as shown in Fig. 10 (d) and (e).

Experiments of ZnO NWs synthesis using microheaters. After the oxidation process, the same parameters are used and experiments are repeated. The synthesized nanowires at time intervals of 1, 2 and 6.5 hours are shown in Figs. 11 (a), (b) and (c), respectively. Both microheaters are operated by applying $4V_{pp}$, 10 kHz heating
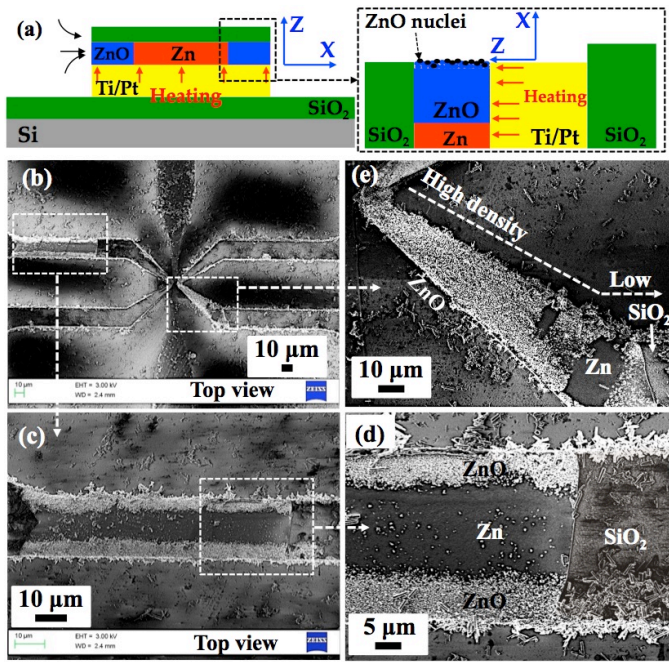
Fig.10 (a) The illustration of Zn layer oxidation under a constraining SiO₂ layer; and (b-e) identification of the oxidised region of the ZnO seed layer by synthesized ZnO NWs.
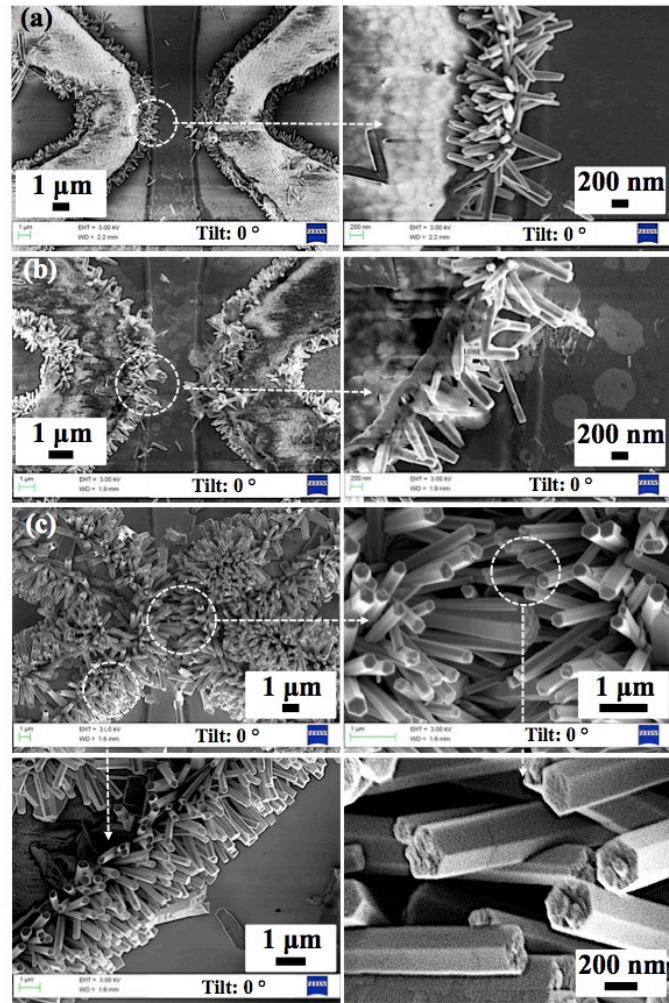
voltage and a further $10V_{pp}$, 10 MHz bias voltages is set to simultaneously align the grown ZnO NWs between two microheaters. After 6.5 hours synthesis, the 500 nm thick SiO₂ constraining layer can still prevent the ZnO NWs being synthesized on the top surface of microheaters. As can be seen from Fig. 11 (c), the growth of ZnO NWs can be controlled well by using this hybrid approach and ZnO NWs are synthesized from the sidewall of the oxidised ZnO seed layer to form transversely suspended nanowires between the two microheaters. Furthermore, the synthesized ZnO NWs are physically in contact as seen in the intermediate section SEM detail in Fig. 11 (c). However, there is still some peeling at the edge of constraining layer, as shown in Fig. 11 (c). This might be caused by the increasing diameter and fresh growth of ZnO NWs over time but it is possible to be eliminated by various treatments, such as reducing the thickness of the ZnO seed layer, adding a capping solution to restrict increase in lateral nanowire dimension and by lowering the concentration of the synthesis solution.

We also tested a single microheater for the synthesis of ZnO NWs without applying the electric field assistance approach. The ZnO NWs presented in Fig. 12 (a) are synthesized on by applying 4Vpp, 10 kHz heating voltage under 20 mM of zinc nitrate and HMTA solution for 8.5 hours. By comparison with Fig. 12 (b), there is no dramatic length increase after 17 hours synthesis. However, the ZnO NWs morphs into ZnO rods as the diameter progressively increases. Furthermore, several ZnO seed grains result on the tip of the ZnO rods towards the end of the process and new ZnO nanostructures grow from these regions, as can be seen in Fig. 12 (b). Unfortunately, it shows that thin SiO₂ constraining layer could not sufficiently prevent vertical growth of ZnO

Fig.11 (a-c) Sequential SEM images of synthesized and aligned ZnO NWs taken at different time intervals.
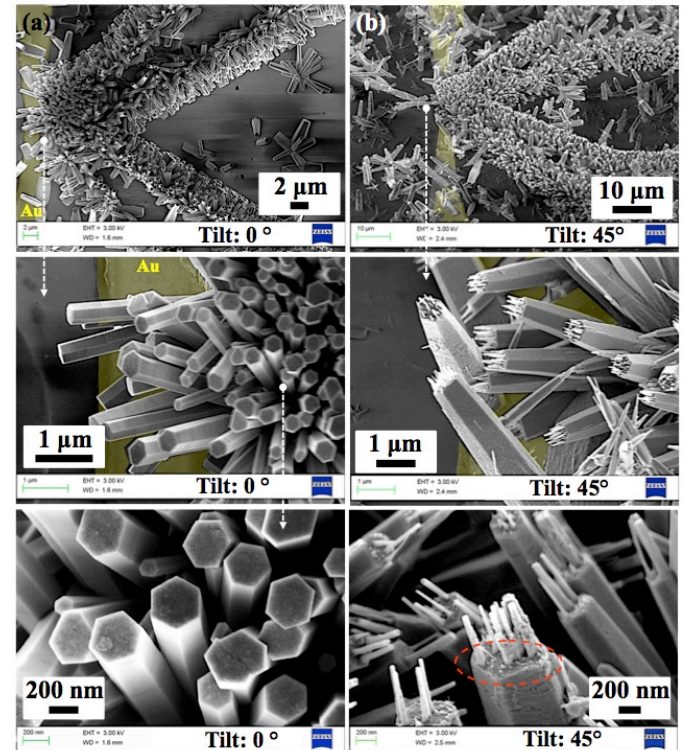

Fig.12 (a) and (b) SEM pictures of the ZnO NWs and hybrid nanorods synthesized after 8.5 hours and 17 hours, respectively.

NWs and peeling occurred from the edge after a long synthesis time. Then, ZnO NWs were synthesised almost on the whole surface of the oxidized ZnO seed layer. Moreover, rough nanocrystalline ZnO seeds anchored on the SiO₂ substrate near the microheater patterns during hydrothermal synthesis.

To investigate the phenomenon of hybrid nanorod synthesis, different concentration-dependent synthesis experiments were conducted. Fig. 13 (a) and (b) provide TEM images of synthesized ZnO nanostructures. The synthesized ZnO nanostructures in Fig. 13 (a) and (b) are synthesized under the 20 mM and 5 mM of the zinc nitrate and HMTA solution for 3 hours, respectively. The low concentration solution is used to simulate the synthesis reaction in the last few hours, as for the experiment presented in Fig. 12 (b). Similarly, several new ZnO seed grains and nanotubes are synthesized on the tip surface of nanorods, as can be seen from Fig. 13 (b). These hybrid ZnO nanotubes and rods are synthesized corresponding following Zn concentration decrease in the synthesis solution. Furthermore, it also clearly shows that the aspect ratio of the synthesized ZnO NWs is affected by the concentration. From the TEM and selected area electron diffraction (SAED) measurements, the crystalline structure of the synthesized ZnO NWs and hybrid ZnO rods with nanotubes can be categorized as hexagonal Wurtzite structure and space group-186.
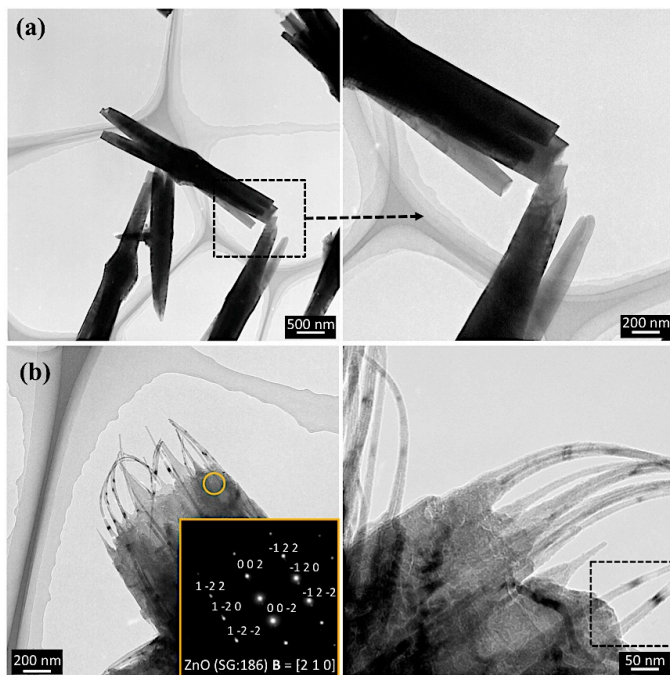

Fig.13 (a) TEM images of ZnO NWs synthesized using 20 mM of zinc nitrate and HMTA synthesis solution; (b) Synthesized hybrid ZnO nanostructures using 5 mM synthesis solution.

Device Case Study. ZnO NWs are sensitive to UV light and this property can be exploited for several applications, such as in photodetectors and chemical sensors. Figure 14 (a) and (b) demonstrate results obtained from I-V characterisation and UV photoresponsivity of the ZnO NWs fabricated using the approach outlined in this work. The I-V property of the device was characterized for bias voltages ranging from -1 V to 1 V under ambient conditions. In the dark condition, the I-V curve was slightly asymmetric and nonlinear, originating from the existence of barriers between the Ti/Pt electrodes and the ZnO NWs [18]. The I-V response showed a current increase from 0.5 mA to 0.8 mA, and then to 1.5 mA at 1 V bias voltage, as the device was subjected to UV radiation of wavelength equal to 254 nm and 365 nm.
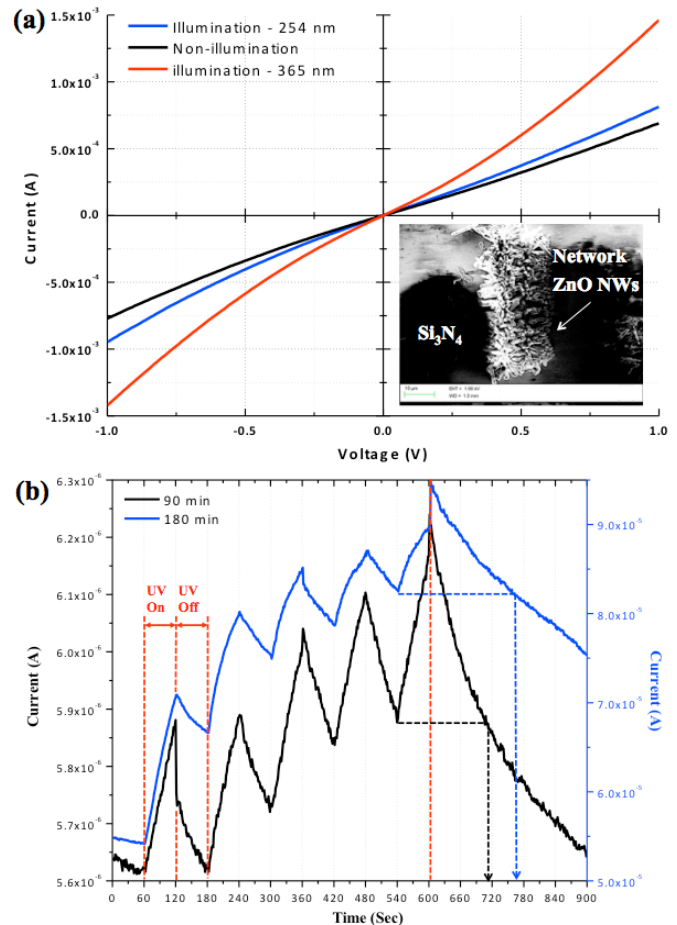

Fig.14 (a) I-V characteristics of the network ZnO NWs device in dark (black line), 254 nm (blue line) and 365 nm (red line) UV illumination; (b) Photo-response characteristics for two different devices by repeatedly switching the UV radiation (365 nm) on and off.

Two more devices (with differing synthesis times of 90 and 180 minutes respectively) were separately tested under the same UV (λ=365 nm) illumination system to characterize photoresponse times, repeatability and response stability over time. Figure 14 (b) presents the response of the two devices where device current is measured as a function of time, when the 365 nm UV light is periodically switched on and off.

IV. CONCLUSION

This paper presents an approach towards the *in-situ* synthesis of ZnO nanostructures based on microheaters. Several issues, including seed layer preparation, local heating synthesis, constraining-layer and electric field directed alignment, and the concentration of synthesis solution, are

investigated to optimize the synthesis procedure. As demonstrated in Fig. 11 (c), transversely suspended ZnO NWs are synthesized and aligned by using this combinative approach between two microheater elements in aqueous solution. Optimal heating and alignment voltages are found (4 V_{pp}, 10 KHz and 10 V_{pp}, 10 MHz respectively) for synthesizing the bridged ZnO NWs and the synthesis is operated under 20 mM of zinc nitrate and HMTA solution for 6.5 hours.

With regard to ZnO seed layer preparation, the appropriate parameters to deposit the initial Zn layer for oxidation to create a ZnO seed layer is 70 W for sputtering resulting in a fine roughness of Zn surface without compound ZnO nanostructures. Then, the Zn layer is fully oxidised by the 10 V_{pp}, 10 KHz applied heating voltage for 10 minutes in the ambient. ZnO NWs are directly synthesized on the oxidised ZnO seed surface by applying 4 V_{pp}, 100 KHz heating voltage under 20 mM of zinc nitrate and HMTA solution for 90 minutes.

Additionally, various thicknesses of SiO_2 constraining layer are studied to constrain ZnO nanowire synthesis to the horizontal direction. To ensure appropriate physical isolation during the synthesis process, the thickness of constraining layer needs to be increased up to 500 nm to operate under the required temperatures. Moreover, an electric field alignment approach is utilised to simultaneously assist ZnO NWs synthesis along with the horizontal direction.

Synthesis is carried out under 5 mM and 20 mM of zinc nitrate and HMTA solution respectively to correlate synthesis conditions to the geometry of the synthesized ZnO nanostructure. During the 17 hour synthesis, several nanotubes and tiny ZnO grains are found to grow on the tip surface of nanorods. TEM and SAED analysis reveal the crystalline structure of the synthesized nanorods and hybrid nanostructures as hexagonal Wurtzite structure and spacing group -186.

Finally, ZnO NW devices fabricated using this approach were characterized as UV photodetector elements. Preliminary experiments were conducted to characterizeI-V response and UV photoresponse under ambient conditions demonstrating the feasibility of the fabrication approach to address practical device applications.

ACKNOWLEDGEMENTS AND NOTES

REFERENCES

[1] Z. L. Wang, "Zinc oxide nanostructures: growth, properties and applications," *Journal of Physics-Condensed Matter,* vol. 16, no. 25, pp. R829-R858, Jun, 2004.

[2] M. A. Khaderbad, Y. Choi, P. Hiralal *et al.*, "Electrical actuation and readout in a nanoelectromechanical resonator based on a laterally suspended zinc oxide nanowire," *Nanotechnology,* vol. 23, no. 2, pp. 025501-1-025501-7, Jan, 2012.

[3] B. E. Alaca, "Integration of one-dimensional nanostructures with microsystems: an overview," *International Materials Reviews,* vol. 54, no. 5, pp. 245-282, Sep, 2009.

[4] M. C. P. Wang, and B. D. Gates, "Directed assembly of nanowires," *Materials Today,* vol. 12, no. 5, pp. 34-43, May, 2009.

[5] J. F. Conley, L. Stecker, and Y. Ono, "Directed integration of ZnO nanobridge devices on a Si substrate," *Applied Physics Letters,* vol. 87, no. 22, pp. 223114-1-223114-3, Nov, 2005.

[6] J. K. Hwang, S. Cho, E. K. Seo *et al.*, "Large-Area Fabrication of Patterned ZnO-Nanowire Arrays Using Light Stamping Lithography," *Acs Applied Materials & Interfaces,* vol. 1, no. 12, pp. 2843-2847, Dec, 2009.

[7] M. W. Li, R. B. Bhiladvala, T. J. Morrow *et al.*, "Bottom-up assembly of large-area nanowire resonator arrays," *Nature Nanotechnology,* vol. 3, no. 2, pp. 88-92, Feb, 2008.

[8] B. D. Sosnowchik, L. Lin, and O. Englander, "Localized heating induced chemical vapor deposition for one-dimensional nanostructure synthesis," *Journal of Applied Physics,* vol. 107, no. 5, pp. 051101-1-051101-14, Mar 1, 2010.

[9] Y. J. Kim, J. M. Jeon, J. H. Choi *et al.*, "ZnO nanostructures with controlled morphologies on a glass substrate," *Nanotechnology,* vol. 21, no. 26, pp. 265603-1-265603-6, Jul, 2010.

[10] T. Hirate, S. Sasaki, W. C. Li *et al.*, "Effects of laser-ablated impurity on aligned ZnO nanorods grown by chemical vapor deposition," *Thin Solid Films,* vol. 487, no. 1-2, pp. 35-39, Sep, 2005.

[11] A. P. Nayak, T. C. Lin, D. Lam *et al.*, "UV and Oxygen Sensing Properties and Space Charge Limited Transport of Sonochemically Grown ZnO Nanowires," *Nanoscience and Nanotechnology Letters,* vol. 4, no. 10, pp. 977-982, Oct, 2012.

[12] V. Pachauri, A. Vlandas, K. Kern *et al.*, "Site-Specific Self-Assembled Liquid-Gated ZnO Nanowire Transistors for Sensing Applications," *Small,* vol. 6, no. 4, pp. 589-594, Feb, 2010.

[13] L. Wei-Chih, Y. Yao-Joe, H. Gen-Wen *et al.*, "Selective local synthesis of nanowires on a microreactor chip," *Sensors and Actuators A (Physical),* vol. 130-131, pp. 625-632632, 14, 2006.

[14] S. Baruah, and J. Dutta, "Hydrothermal growth of ZnO nanostructures," *Science and Technology of Advanced Materials,* vol. 10, no. 1, pp. 013001-1-013001-18, Mar, 2009.

[15] W. C. Lin, Y. C. Lin, C. J. Shih *et al.*, "Local synthesis and alignment of zinc oxide nanowires in aqueous solution using microheaters," *2012 IEEE 25th International Conference on Micro Electro Mechanical Systems (MEMS)*, pp. 452-455455, 2012, 2012.

[16] L. Weichih, A. A. Seshia, W. Ching-Chen *et al.*, "Catalyst-free synthesis of zinc oxide nanostructures by microheaters in the ambient environment," *Proceedings of the 2011 6th IEEE International Conference on Nano/Micro Engineered and Molecular Systems (NEMS 2011)*, pp. 897-900900, 2011, 2011.

[17] K. A. Alim, V. A. Fonoberov, M. Shamsa *et al.*, "Micro-Raman investigation of optical phonons in ZnO nanocrystals," *Journal of Applied Physics,* vol. 97, no. 12, pp. 223114-1- 223114-3, Jun 15, 2005.

[18] Z. M. Liao, J. Xu, J. M. Zhang *et al.*, "Photovoltaic effect and charge storage in single ZnO nanowires," *Applied Physics Letters,* vol. 93, no. 2, pp. 1-3, Jul, 2008.